Materials and Design 46 (2013) 660–667

Contents lists available at SciVerse ScienceDirect

Materials and Design

journal homepage: www.elsevier.com/locate/matdes

Technical Report

Microstructures and mechanical properties of creep resistant steel for application at elevated temperatures

Lj. Milović [a,*], T. Vuherer [b], I. Blačić [c], M. Vrhovac [d], M. Stanković [e]

[a] Faculty of Technology and Metallurgy, University of Belgrade, Karnegijeva 4, 11120 Belgrade, Serbia
[b] Faculty of Mechanical Engineering, University of Maribor, Smetanova 17, 2000 Maribor, Slovenia
[c] Military Technical Institute, Ratka Resanovića 1, 11030 Belgrade, Serbia
[d] Instituto de Soldadura e Qualidade ISQ, Taguspark-Oeiras, Av. Prof. Dr. Cavaco Silva 33, 2740-120 Porto Salvo, Portugal
[e] Innovation Center, Faculty of Mechanical Engineering, University of Belgrade, Kraljice Marije 16, 11120 Belgrade, Serbia

ARTICLE INFO

Article history:
Received 21 August 2012
Accepted 31 October 2012
Available online 23 November 2012

ABSTRACT

The subject of this paper is the microstructural and mechanical characterisation of regions of the heat-affected zone (HAZ) in steels containing 9–12% Cr that are used for operation at elevated temperatures. Tests were performed on regions in the HAZ, which was created by physical simulation using a thermal welding simulator. Half of the simulated samples (SSs) were tested at room temperature (RT) and at an operating temperature (OT) of 600 °C immediately after simulation/welding, while the rest of the simulated samples were tested at RT and at the OT after heat treatment following the welding, i.e., post-weld heat treatment (PWHT). In addition to the results from mechanical testing, the results from microstructural analysis using light microscopy, scanning electron microscopy (SEM) and transmission electron microscopy (TEM) are also presented. The manner in which PWHT contributes to the creep resistance of the HAZ in P91 steel is demonstrated.

1. Introduction

The components built into modern fossil-fuel power stations are made of ferritic steels containing 1–12 wt.% Cr and 0.5–1 wt.% Mo, which are designed for an OT of up to 600 °C. The need to reduce CO_2 emissions and to increase the efficiency of power stations (by increasing steam operating pressures and temperatures) led to a modification of these steels. Namely, these materials, known as T/P91 steels (9Cr-1 Mo–NbV), are not used for operating temperatures (OTs) above 600 °C, as they do not possess the required creep strength and oxidation resistance at elevated temperatures. Impressive progress has been made in the analysis of the specific microstructural instability that causes a loss in creep strength at an OT of 550 °C and above, including the prediction of the onset time of the creep strength loss and theoretical modelling of precipitation sequences in power plant steels. New types of highly creep-resistant bainitic 3Cr and martensitic 9–12Cr, such as T23 and P92 steels, with higher creep rupture strengths than existing steels are already being developed [1].

The problems encountered in welded joints (WJ) of T/P91 steel under creep conditions [2–4], both in parent metal (PM) and weld metal (WM), are the result of Type IV cracking, i.e., crack initiation in the region of the heat-affected zone (HAZ) immediately next to the PM. Specifically, Type IV cracking may occur either in an intercritical HAZ (ICHAZ), i.e., in the region of the HAZ heated to a maximum temperature $A_{c1} < T_p < A_{c3}$, or in a fine-grained HAZ (FGHAZ), i.e., in the region of the HAZ heated slightly above A_{c3}. The initiation of cracks of this type is mostly affected by microstructural variations during welding, post-weld heat treatment (PWHT) and service or creep tests [5–9]. HAZ material exhibiting a fine-grained structure showed the lowest creep strength. Coarse-grained WM generally had the highest creep strength, whereas PM exhibited an intermediate behaviour [10,11].

Due to advanced transmission electron microscopy (TEM) specimen preparations, the former location of extracted particles, such as on grain/lath/subgrain boundaries, can be determined before microanalysis [12,13]. The most significant factors in reducing the creep rupture strength of the FGHAZ of WJ in P91 steel, as compared with the CGHAZ of WJ and PM, are as follows: the finer prior austenite grain size in the fine grained region, which accelerates the rate of growth of martensite lath sub grains and enhances creep cavitations, and the lower peak temperature during welding, which results in a softer martensite matrix [14]. Additionally, chromium-rich martensite laths play the largest role in the oxidation process at an elevated OT by enhancing the chromium flux from the metal towards the surface [15,16].

PWHT of the as-welded joints made from modified 9Cr-1 Mo steel is necessary in fabricating the high-temperature structural

* Corresponding author. Address: Karnegijeva 4, 11120 Beograd, Srbija. Tel.: +381 63 8124 965; fax: +381 11 3370 387.
E-mail addresses: acibulj@tmf.bg.ac.rs (Lj. Milović), tomaz.vuherer@uni-mb.si (T. Vuherer), ivo.blacic@gmail.com (I. Blačić), mvrhovac@clix.pt (M. Vrhovac), shomyguca@yahoo.com (M. Stanković).

0261-3069/$ - see front matter © 2012 Elsevier Ltd. All rights reserved.
http://dx.doi.org/10.1016/j.matdes.2012.10.057

components of steam power plants. The recovery and recrystallisation occurring at 730 °C, held for 2 h led to the fragmentation of martensite laths and thus to the formation of equiaxial grains. Variation in the recovery and recrystallisation behaviours is largely influenced by the distribution of the $M_{23}C_6$ precipitates in the microstructure of the modified 9Cr-1 Mo steel weldments after PWHT [17]. The literature shows that analytical testing using TEM at characteristic spots during a certain cycle of welding and subsequent PWHT shows the complete dissolution of precipitates, i.e., Cr-carbides, V-nitrides and (Nb,V), and of (C,N) during the thermal welding cycle. During PWHT, they precipitate again and are distributed similarly to the precipitates in the initial PM [18–22]. Advanced microstructural characterisation has demonstrated that long-term microstructural stability in 9–12% Cr steels under technical loading conditions is related to the precipitate stability. Mo and W can have a positive influence on the long-term creep strength of 9–12% Cr steels by Laves phase precipitation hardening. The unexpected breakdown of the long-term creep stability of a number of alloys is due to the precipitation of the complex Z-phase nitride, which may completely dissolve fine V- and Nb-containing MX nitrides. High Cr contents of 10% and above in these steels accelerate the Z-phase precipitation [23]. Although such steels normally have a fully martensitic microstructure, they are susceptible to the formation of delta ferrite, mainly during the welding process. Delta ferrite has several detrimental effects on properties such as creep, ductility and toughness. Thus, it is important to avoid its formation. The most effective way to avoid delta ferrite in the WM, in order to obtain a fully martensitic microstructure, is to reduce the amount of ferrite forming elements to as low a concentration as possible. The partial substitution of Mo for W helps austenite stability and would be expected to improve the mechanical properties at high temperature [24].

In this investigation, three states of a P91 material were tested: the PM (initial structure of the material), the simulated HAZ region at 925 °C without PWHT (SS925, no. PWHT), and the simulated HAZ region at 925 °C with PWHT (SS925 PWHT). The simulated HAZ region at T_p = 925 °C was marked by testing as a region where Type IV cracking could occur, which is shown in [21,22,25] in detail. Considering the loading of steam line components, the data on the behaviour of the HAZ of WJ were obtained by tensile testing of smooth specimens and by testing of specimens in the notched regions. The PM samples and the samples obtained by the simulation of welding (SS) of virgin material were tested. The PM and SS were tested to determine the chemical composition, hardness, structure, microstructure, tensile properties and impact energy at a room temperature (RT) of 20 °C and at an OT of 600 °C.

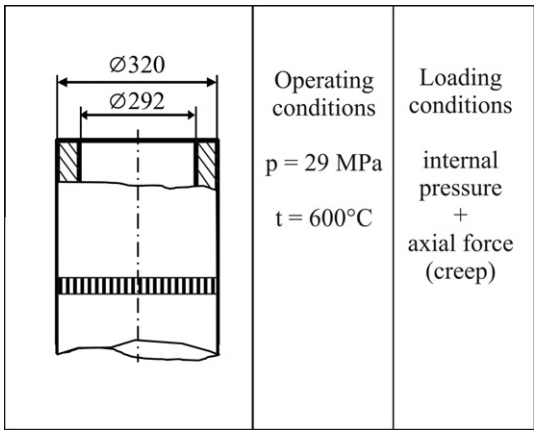

Fig. 1. Dimensions of the tested pipe and operating conditions.

Table 1
Chemical composition of the tested material, wt.%.

C	Si	Mn	P	S	Cr
0.120	0.289	0.396	0.009	0.002	8.04
Ni	Cu	Al	Mo	Ti	As
0.080	0.082	0.024	0.850	0.003	0.007
V	Nb	W	Sb	Co	N
0.242	0.073	0.013	0.0091	0.012	0.040

Table 2
Mechanical properties of the PM.

R_m (MPa)	$R_{p0.2}$ (MPa)	E (GPa)	A_5 (%)	E_{tot} (J)
720	560	211	21	196

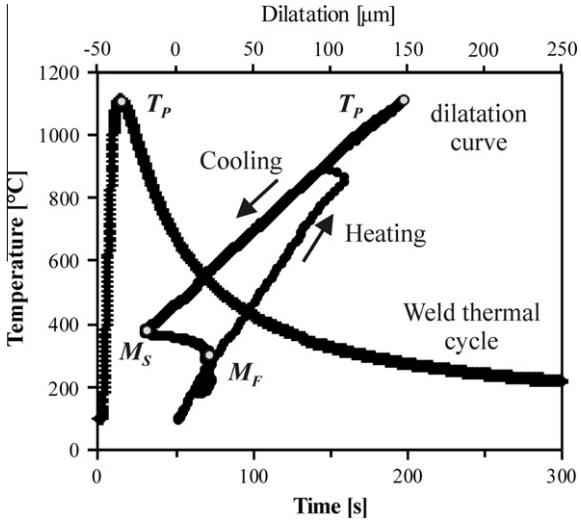

Fig. 2. Welding thermal cycle curve and dilatometric curve.

Table 3
Simulation parameters for the tested material.

T_p (°C)	$\Delta t_{8/5}$ (°C)	T_{hold} (°C)	t_{hold} (s)
1386	40	1386	0.5
1300	40	1300	0.5
1250	40	1250	0.5
1200	40	1200	0.5
1150	40	1150	0.5
1100	40	1100	0.5
1050	40	1050	0.5
1000	40	1000	0.5
950	40	950	0.5
925	40	925	0.5
900	40	900	0.5
850	40	850	0.5

2. Literature data on the P91 steels microstructure

The 9–12% chromium heat resistant steels have a complex microstructure that consists of fine micro grains that are separated by a variety of different interfaces (prior austenite grain boundaries, block boundaries, twin boundaries and sub grain boundaries) and of carbides that are precipitated on or near these boundaries [26]. P91 steels are heat treated to produce a martensitic microstructure that is subsequently tempered to improve the ductility and impact strength at elevated temperatures. The heat treatment consists of austenitisation at temperatures of approximately

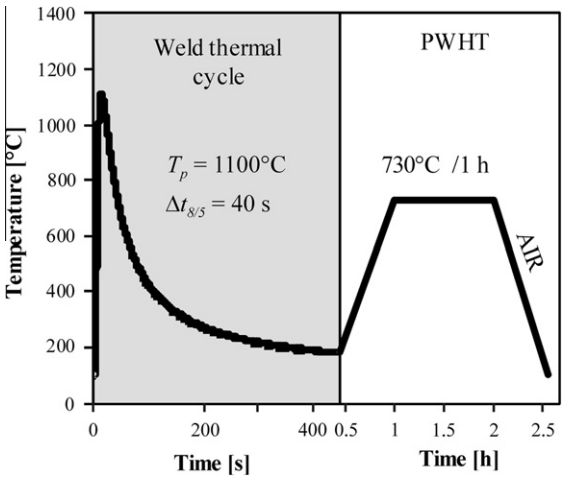

Fig. 3. Schematic of the welding thermal cycle and PWHT.

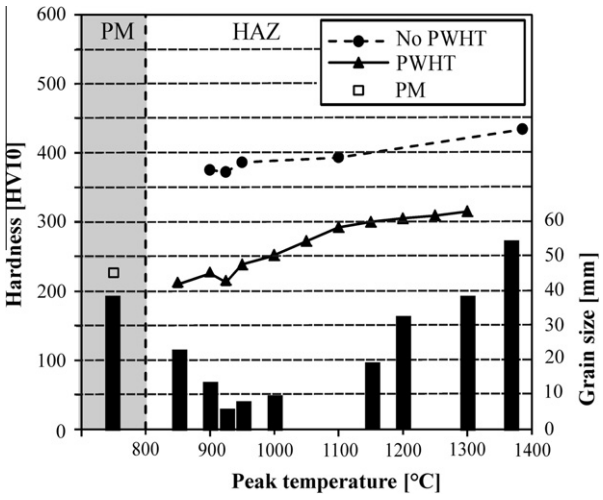

Fig. 4. Hardness of the PM and SS before and after PWHT, and the grain sizes of the SS.

1100 °C, quenching and high temperature tempering at approximately 750 °C. Austenitising produced a martensitic structure with a high dislocation density within the martensite laths. During tempering, recovery caused the formation of sub grains and of dislocation networks. By using heat treatment, a good combination of impact strength, ductility and creep strength during use can be achieved. Creep strength is inversely correlated with the martensite lath width and with the sub grain size [5].

In steels, chromium delays the formation of carbides. After heat-treatment, the mechanical strength of P91 steels is improved as a result of the precipitation and homogeneous distribution of V and Cr originating from the carbides. Two types of precipitates can be found in 9–12% chromium heat resistant steels: $M_{23}C_6$ carbides (M = Cr, Fe or Mo), located at the prior austenite grain boundaries and at other boundaries, and finely dispersed MX-type carbonitrides (M = V, Nb and X = C, N) within the martensite laths. The MX precipitates restrain the movement of dislocations by anchoring them and, therefore, provide high resistance to creep. The optimum range of austenitising temperatures (680–780 °C) is adjusted so that the $M_{23}C_6$ carbides and MX carbonitrides could dissolve into a solid solution. NbC carbides should remain undissolved in austenite to form austenite fine grains, which will have a favourable influence on the ductile properties [26,27].

3. Experimental details

3.1. Materials

The tested pipe (Fig. 1) was made of P91 steel. P91 steel is martensitic, case hardened, high-chromium steel used for operation at elevated temperatures and under high pressures and was built into components for steam lines of thermal power plants. The chemical composition of the tested material is given in Table 1 while the measured values of the tensile properties are given in Table 2.

3.2. HAZ microstructure simulation

Physical HAZ simulation procedures, which are commonly used, were applied to the PM in laboratory conditions in order to characterise in detail the different regions within the HAZ of a welded

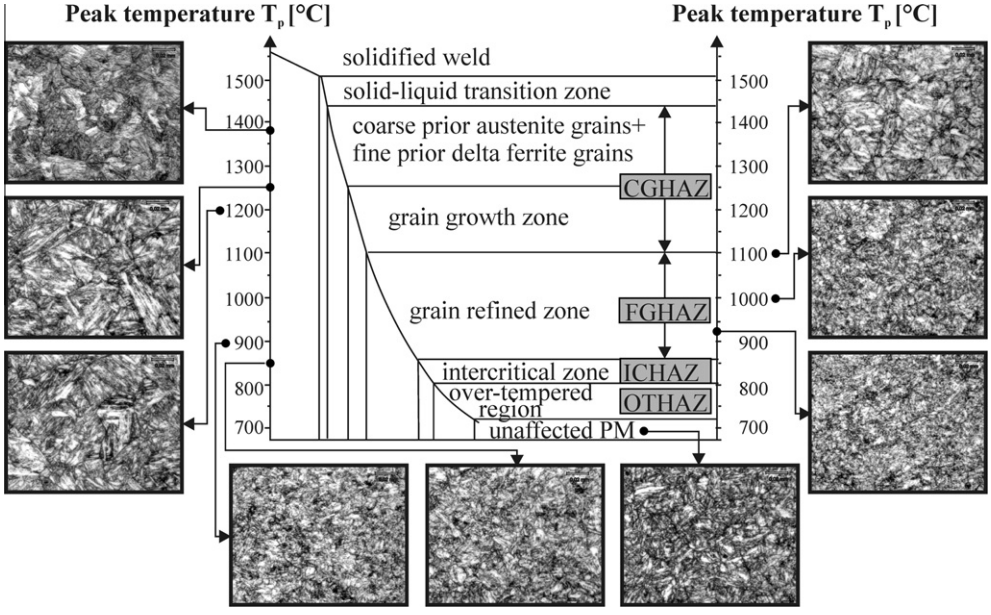

Fig. 5. Microstructure of some regions of the simulated HAZ: CG-coarse grain, FG-fine grain, IC-intercritical, OT-over tempered.

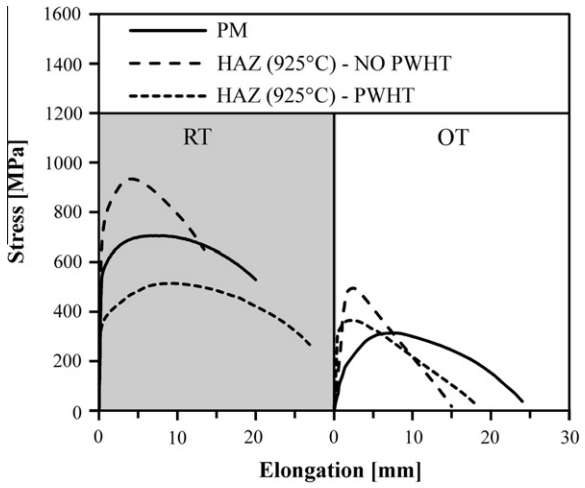

Fig. 6. Tensile properties of the PM and SS at RT and at the OT.

joint. The physical simulation of HAZ involves the exact reproduction of the thermal and mechanical conditions that the material would be subjected to in the actual welding process. A small sample of the material, which exhibits the same thermal and mechanical profile as it would in the full scale welding process, was used in the physical simulation.

For simulation of the HAZ microstructure, the thermal welding simulator SMITWELD 1405 and specimens with square cross sections of 11 × 11 × 70 mm were used. The thermal welding cycles needed for simulation were estimated based on actual thermal cycles measured during welding.

Characteristic transformation temperatures during the welding cycle were determined from the dilatometric curve and are A_{c1} = 835 °C and A_{c3} = 930 °C. The heating rate was 53.8 °C/s. The temperature of the onset of the martensite formation was M_s = 375 °C, and the transformation of martensite was completed by the temperature M_f = 210 °C (Fig. 2). The formation of martensite was preceded by the separation of a small quantity of bainite. Different regions of the HAZ were obtained by simulation of single-pass welding at 12 different temperatures with the cooling time $\Delta t_{8/5}$ = 40 s, [21]. In Table 3, a detailed survey of the simulation modes for a sample is given. To test the influence of PWHT on the HAZ microstructure, after welding all samples were subjected to PWHT at 730 °C for 1 h and then air-cooled (Fig. 3).

4. Results and discussions

For all samples, the hardness and grain size were measured (Fig. 4), and the microstructure was examined (Fig. 5). Additionally, the tensile properties of tested material were determined from round specimens taken from SS, the dimensions of which were Ø5 × 70 mm. Tensile tests at an OT of 600 °C were conducted in a high temperature chamber, where the loading rate was 5 mm/min. The results for the tensile properties are given in Fig. 6. Diagrams were obtained from the testing of the impact energy using an instrumented Charpy pendulum, from which the energy necessary for crack initiation and crack propagation and the total impact energy were determined. The results of the impact tests and the appearances of obtained fracture surfaces are shown in Fig. 7.

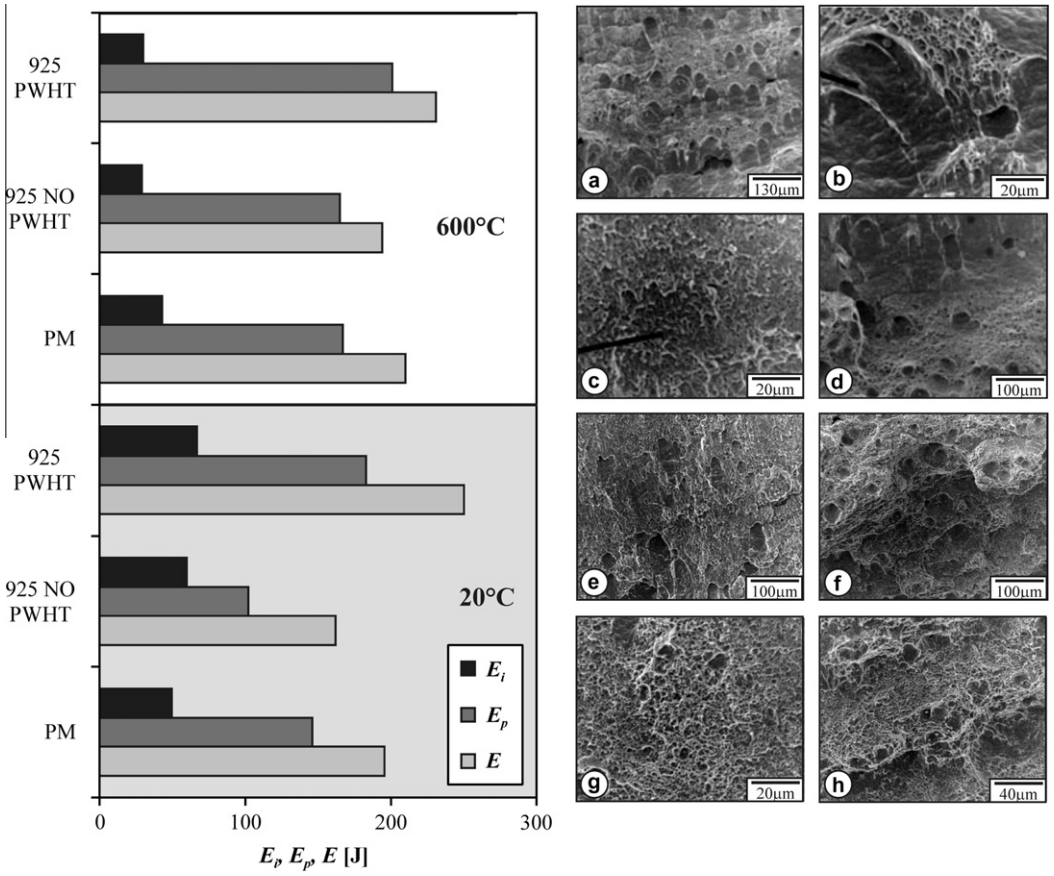

Fig. 7. Distribution of the total impact energy (E), crack-initiation energy (E_i) and crack-propagation energy (E_p) in the PM and SS as well as the appearance of fracture surfaces of the SS: (a) and (b) SS PWHT at 600 °C, (c) and (d) SS no PWHT at 600 °C, (e) and (f) SS PWHT at 20 °C, (g) and (h) SS no. PWHT at 20 °C.

Table 4
Grain size and martensite-packet size in the region of CGHAZ.

Simulation temperature T_p (°C)	Grain mean diameter (μm)	Size of martensite packets (μm)
1386	53.4	18.25
1300	37.8	15.33
1200	31.8	13.95
1150	18.9	12.12

4.1. Effect of the austenising conditions

The microstructures of the PM and simulated regions in the HAZ are shown in Fig. 5. The PM structure consisted of tempered lath martensite. In the HAZ regions with a fine-grain structure (OTHAZ and ICHAZ), i.e., at simulation temperatures of 850 °C < T_p < 925 °C, the structure of the PM originally consisting of tempered martensite partially transformed into austenite that again transformed into martensite during cooling following simulation. This martensite was subsequently tempered during PWHT. Therefore, the resulting microstructure consisted of tempered martensite of the PM and of tempered martensite formed during simulation. The fraction of formed austenite increased with a rise in the simulation temperature, so at T_p = 925 °C the fraction was 90%, which was determined using the dilatometric curve (Fig. 2).

Up to T_p = 1100 °C (the beginning of the CGHAZ region), the grain size was homogeneous, and the grain growth was controlled by precipitates VN and NbN [23,24]. In the CGHAZ region, one can observe that the grain size varies, which is the consequence of incomplete recrystallisation. As one can see from Table 4, the grain size increases with the rise in T_p and, at the same time, the size of martensitic packets increases as well.

The inspection of all simulated HAZ regions shows that the smallest grain size occurred at T_p = 925 °C, which is why this temperature was selected to characterise the zone where Type IV cracks could initiate under creep conditions [28–30].

4.2. Characterisation of the PM

A TEM micrograph of the PM is shown in Fig. 8. The PM consists of tempered lath martensite with elongated carbides at the laths' boundaries and individual dislocations within the laths (Fig. 8a). In Fig. 8b, a carbide at the triple boundary and a precipitate separated at the lath boundary has been observed. The boundaries are clearly visible, which indicate that there is no stress at the boundaries (because the material was tempered during the production process). The MX type precipitates within laths and the elongated carbides at the laths' boundaries are shown in Fig. 8c.

4.3. Characterisation of the FGHAZ

The region of T_p = 925 °C, i.e., the region where Type IV cracks could initiate under creep conditions, was measured using TEM after simulation without PWHT (Fig. 9) and after subsequent PWHT (Fig. 10). Prior-austenite grains of 4 μm, in which one can observe the packets of martensite, is shown in Fig. 9a. In Fig. 9b, the martensite laths with no carbides separated at the laths' boundaries are shown. The laths' boundaries are less prominent and the dislocation density is higher within the laths, which indicates that the strain within the laths is higher than in the case of the PM.

4.4. Effect of tempering

The microstructure in the region of the HAZ after PWHT obtained using scanning electron microscopy (SEM) is shown in Fig. 10a. The presence of particles approximately 1 μm in diameter is observed at prior-austenite grain boundaries. Energy-dispersive spectroscopy (EDS) analysis shows that these particles have a higher content of C, Cr and Mo in comparison with the matrix, Fig. 10c and d; therefore, these are most likely carbides of $M_{23}C_6$ type (M = Cr, Fe, Mo), [26,27]. One can also notice that the carbides separated at the boundaries of former austenitic grains are coarser

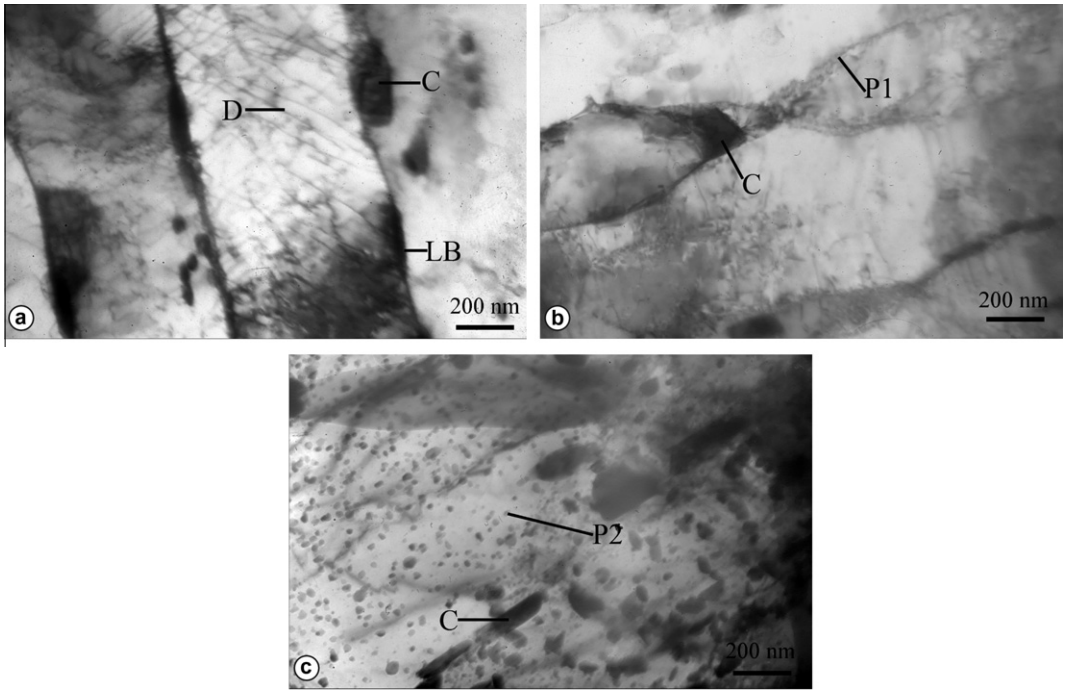

Fig. 8. Microstructure of the PM (TEM micrographs): (a) martensite laths with dislocations – D within laths and carbides – C at lath boundaries – LB, (b) a carbide – C at the triple lath boundary and a precipitate at the lath boundary – P1, and (c) carbides – C at lath boundaries and precipitates within laths – P2.

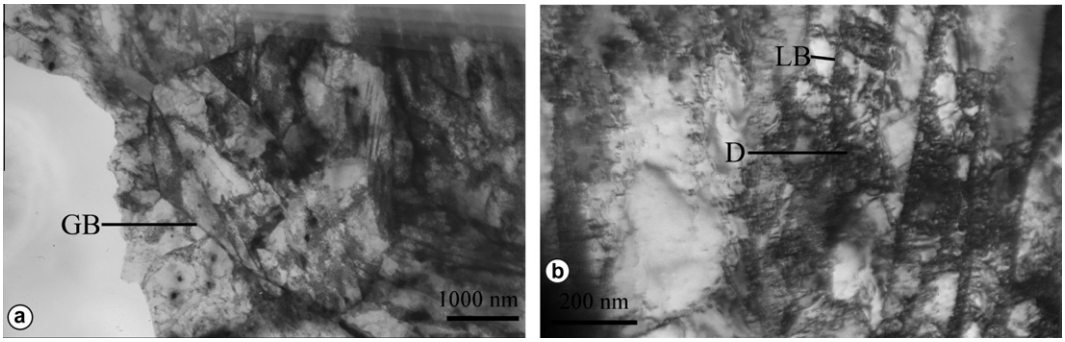

Fig. 9. Microstructure of the SS no PWHT (TEM micrographs): (a) GB – boundaries of prior austenitic grain of 4 μm, and (b) LB – martensitic lath boundaries containing dislocations – D.

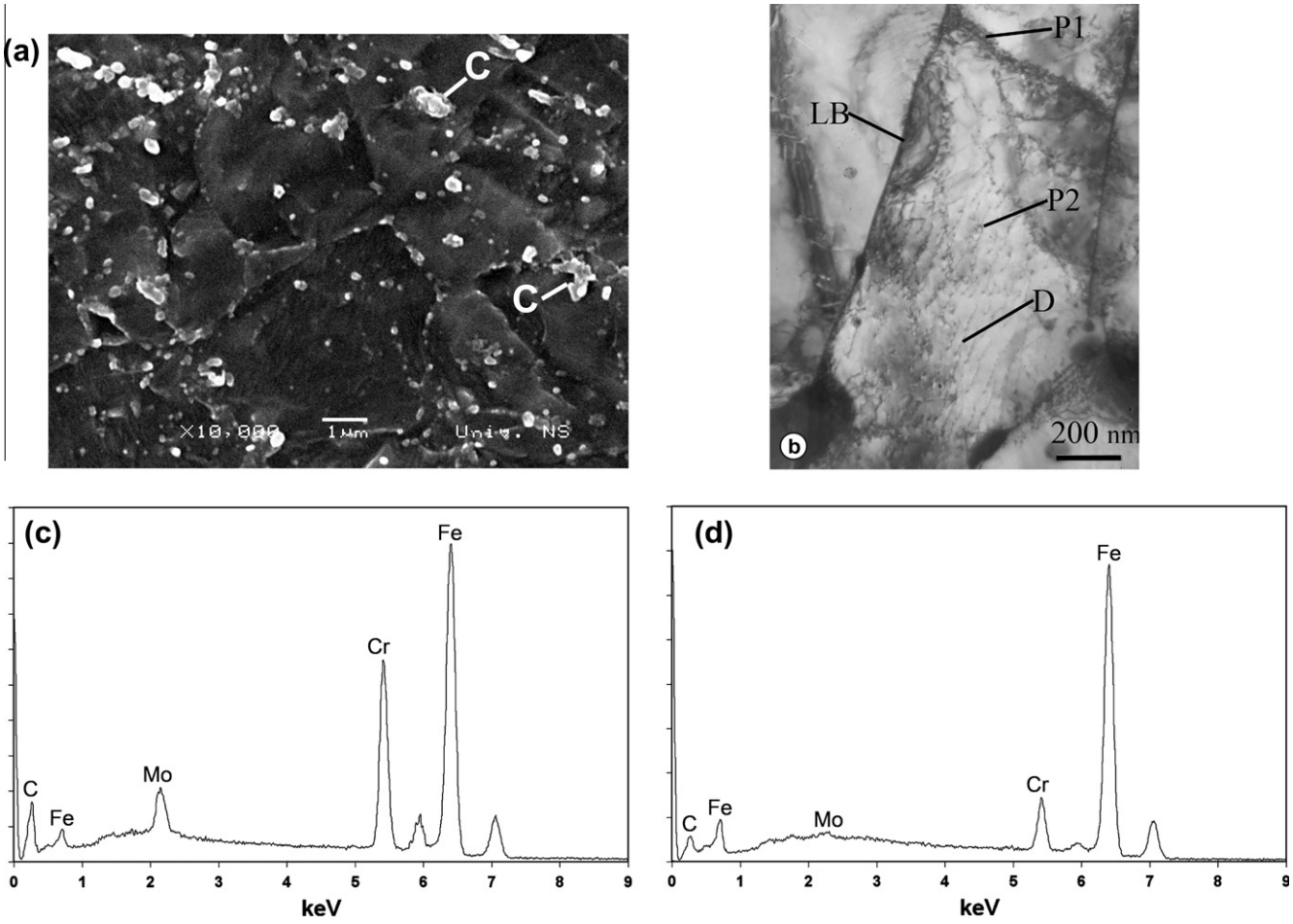

Fig. 10. Microstructure of the SS with PWHT (a) SEM micrograph, C – carbides; (b) TEM micrograph: LB – laths' boundaries, D - dislocations, P1 – precipitates at martensite laths' boundaries, P2 – precipitates within martensite laths; (c) typical EDS spectra of bigger particles; and (d) EDS spectra of the matrix.

than those separated at the boundaries of ferritic sub grains. The microstructure of the SS after PWHT obtained using TEM is shown in Fig. 10b. One can see that the precipitates are more equiaxial and distributed both at the boundaries of martensite laths and within them. The laths' boundaries are clearly visible, which indicates that there is no stress within the grains. The martensite laths gradually disappear and more equiaxial grains appear. The dislocation density within the laths is lower than in the SS without PWHT, which is the consequence of tempering during PWHT.

4.5. Mechanical properties of the HAZ constituents

4.5.1. Hardness

The measured hardness of the PM is 229 HV1 (Fig. 4). The measured hardness of the SS with PWHT is 213 HV1. In the ICHAZ, a substantial drop in the hardness occurs. At this temperature, there is no noticeable dissolution of carbides or nitrides, and there is a transformation of C and N into a solid austenitic solution, which is why martensite formed during cooling has a lower content of

C and N. Due to the lower content of C and N, repeated separation of $M_{23}C_6$ type carbides and of MX type carbonitrides is limited during subsequent heat treatment, and so a lower hardness than that of the PM is obtained (210 HV1). Additionally, MX type carbonitrides coarsen and coagulate, which reduce their hardening effect, causing the lowest hardness in the FGHAZ region. When the temperature of simulation increases, the solubility of carbides also increases; this leads to the increase in the hardness of the CGHAZ.

4.5.2. Tensile properties

At the OT, the yield stress of the SS with PWHT (295 MPa) is higher than the yield stress of the PM (231 MPa), so the strength of welded structural components made of P91 steel will not be jeopardised (Fig. 6).

4.5.3. Impact energy

The values of the total impact energy, E, crack-initiation energy, E_i, and crack-propagation energy, E_p, of the PM and SS with and without PWHT at RT and at OT, as well as the appearance of relevant fracture surfaces of the SS, are shown in Fig. 7.

At RT, the crack-initiation energy, E_i, and crack-propagation energy, E_p, of the SS with PWHT are higher than that of the SS without PWHT. At RT, the crack growth in the SS without PWHT was unstable, Fig. 7g.

At an OT of 600 °C, the total impact energy, E, and crack-propagation energy, E_p, are higher for the SS with PWHT. However, the crack-initiation energy, E_i, is slightly higher for the SS without PWHT.

On the fracture surface of the SS with PWHT at 20 °C (Fig. 7e and f), one can observe less prominent, larger, tearing-induced pits, while at the very top one can observe equiaxial pits, which is the result of higher strength and lower ductility. On the fracture surface (Fig. 7a and b) of the SS with PWHT at 600 °C (the sample with the highest crack-propagation energy E_p = 208 J), one can observe the micro mechanism of the crack propagation exclusively through the tearing-induced pits, which are typical for very ductile states.

On the fracture surface of the SS without PWHT at 20 °C (Fig. 7g and h), one can observe tearing at the crack tip and at the fibre-type zone with equiaxial pits between shear-induced pits. The micro mechanism of quasi-tearing with instable crack growth is noticeable. Brittle behaviour of the material, which leads to instable crack growth, must be avoided as the crack-containing component is susceptible to sudden fracture at cold start or during cooling after shutting down (whether the fracture is caused by a metallurgical defect or by a crack formed during exploitation).

As for the SS without PWHT at 600 °C (Fig. 7c and d), the crack-propagation energy E_p = 165 J is lower than that of the SS with PWHT, which is E_p = 208 J. On the fracture surfaces, one can notice the region with prevailing shear pits and a transition spot between tear-pits and equiaxial pits.

5. Conclusions

The FGHAZ microstructure proved to be the weakest under creep conditions because of the higher tendency towards recrystallisation in this area, which, in relation to the over aging of the precipitates, results in a significant softening of these fine grained zones in the HAZ (which were heated up to 900–950 °C during the weld thermal cycle after PWHT). Based on the inspection of the microstructures of all simulated HAZ regions and the hardness measurements, one can see that the finest grain size was obtained in the soft zone simulated at T_p = 925 °C, which is why this temperature has been chosen to characterise the zone where Type IV cracks can initiate under creep-conditions.

In the present paper, the effects of heat treatment after welding on the microstructure and hardness of some HAZ constituents in P91 steel has been presented. Based on the results from testing, the following conclusions can be drawn:

1. In the HAZ region where Type IV cracks can initiate, which was not subjected to PWHT after simulation/welding, no presence of precipitates at the martensitic lath boundaries was observed, and so the resistance to plastic deformation at the grain boundary is lower.
2. In the HAZ region that was subjected to subsequent PWHT, a precipitate was observed at the boundaries of martensitic laths, which increases the resistance to plastic deformation at lath boundaries, thus increasing the resistance to creep as well.
3. Testing of the impact energy has not shown any essential differences between the values of the energies obtained, in either the crack-initiation or crack propagation energy, especially considering that the values obtained for the energies were relatively high.
4. Fractographic analysis indicated a partially brittle behaviour of the material in the HAZ region without subsequent PWHT after simulation/welding, which is more noticeable at room temperature than at elevated temperatures. This finding suggests the possibility of an instable brittle fracture, mainly caused by the effects of residual tensile stresses and the presence of metallurgical defects; this fracture is particularly likely at cold start or during cooling of welded components. This analysis confirms the recommendation that PWHT should be conducted immediately after welding, before the welded joint cools to below the temperature where formation of martensite is completed.

Acknowledgements

This work is a contribution to the Ministry of Education, Science and Technological Development of the Republic of Serbia funded Project TR 35011. Furthermore, we would like to thank our colleague Tamara Radetić, PhD for the assistance with TEM and Professor Nenad Gubeljak for donating the tested pipe.

References

[1] Abe F. Bainitic and martensitic creep-resistant steels. Curr Opin Solid State Mater Sci 2004;8:305–11.
[2] Abe F. Stress to produce a minimum creep rate of 10–5%/h and stress to cause rupture at 105 h for ferritic and austenitic steels and superalloys. Int J Press Vessels Pip 2008;85:99–107.
[3] Dimmler G, Weinert P, Cerjak H. Extrapolation of short-term creep rupture data-the potential risk of over-estimation. Int J Press Vessels Pip 2008;85:55–62.
[4] Wilshire B, Burt H. Damage evolution during creep of steels. Int J Press Vessels Pip 2008;85:47–54.
[5] Ennis PJ, Czyrska-Filemonowicz A. Recent advances in creep resistant steels for power plant applications. OMMI 2002;1:1–28.
[6] Czyrska-Filemonowicz A, Zielińska-Lipiec A, Ennis PJ. Modified 9% Cr steels for advanced power generation: microstructure and properties. J Achievements Mater Manuf Eng 2006;19:43–8.
[7] Albert SK, Matsui M, Watanabe T, Hongo H, Kubo K, Tabuchi M. Microstructural investigations on Type IV cracking in a high Cr steel. ISIJ Int 2002;42:1497–504.
[8] Francis JA, Mazur W, Bhadeshia HKDH. Type IV cracking in ferritic power plant steels. Mater Sci Technol 2006;22:1387–95.
[9] Tezuka H, Sakurai T. A trigger of Type IV damage and a new heat treatment procedure to suppress it. Microstructural investigations of long-term ex-service Cr–Mo steel pipe elbows. Int J Press Vessels Pip 2005;82:165–74.
[10] Zhao L, Jing H, Xu L, An J, Xiao G. Numerical investigation of factors affecting creep damage accumulation in ASME P92 steel welded joint. Mater Des 2012;34:566–75.
[11] Spigarelli S, Quadrini E. Analysis of the creep behaviour of modified P91 (9Cr-1 Mo–NbV) welds. Mater Des 2002;23:547–52.
[12] Mitchell DRG, Sulaiman S. Advanced TEM specimen preparation methods for replication of P91 steel. Mater Charact 2006;56:49–58.

[13] Kitahara H et al. Crystallographic features of lath martensite in low-carbon steel. Acta Mater 2006;54:1279–88.
[14] Abd El-Azim ME, Nasreldin AM, Zies G, Klenk A. Microstructural instability of a welded joint in P91 steel during creep at 600 °C. Mater Sci Technol 2005;21:779–90.
[15] Tökei Zs, Viefhaus H, Grabke HJ. Initial stages of oxidation of 9Cr Mo V-steel: role of segregation and martensite laths. Appl Surf Sci 2000;165:23–33.
[16] Yajing L, Juan W, Bing Z, Tao F. XRD and TEM analysis of microstructure in the welding zone of 9Cr-1 Mo–V–Nb heat-resisting steel. Bull Mater Sci 2002;25:213–7.
[17] Gao Q, Di X, Liu Y, Yan Z. Recovery and recrystallization in modified 9Cr-1 Mo steel weldments after post-weld heat treatment. Int J Press Vessels Pip 2012;93–94:69–74.
[18] Pešička J, Kužel R, Dronhofer A, Eggeler G. The evolution of dislocation density during heat treatment and creep of tempered martensite ferritic steels. Acta Mater 2003;51:4847–62.
[19] Golański G. Effect of the heat treatment on the structure and properties of GX12CrMoVNbN9-1 cast steel. Arch Mater Sci Eng 2010;46:88–97.
[20] Łomozik M, Zielińska-Lipiec A. Microscopic analysis of the influence of multiple thermal cycles on simulated HAZ toughness in P91 steel. Arch Metall Mater 2008;53:1025–34.
[21] Lj Milović. Microstructural investigations of the simulated heat affected zone of the creep resistant steel P91. Mater High Temp 2010;27:233–42.
[22] Milović Lj, Vuherer T, Zrilić M, Sedmak A, Putić S. Study of the simulated heat affected zone of creep resistant 9–12% advanced chromium steel. Mater Manuf Processes 2008;23:597–602.
[23] Hald J. Microstructure and long-term creep properties of 9–12% Cr steels. Int J Press Vessels Pip 2008;85:30–7.
[24] Oñoro J. Weld metal microstructure analysis of 9–12% Cr steels. Int J Press Vessels Pip 2006;83:540–5.
[25] Milović, Lj. The analysis of integrity of welded components of processing equipment for elevated operating temperatures. D.Sc. thesis; University of Belgrade; 2008 [in Serbian].
[26] Panait C, Bendick W, Fuchsmann A, Gourgues-Lorenzon A-F, Besson J. Study of the microstructure of the grade 91 steel after more than 100,000 h of creep exposure at 600 °C. Int J Press Vessels Pip 2010;87:326–35.
[27] Kaneko K, Matsumura S, Sadakata A, Fujita K, Moon W-J, Ozaki S, et al. Characterization of carbides at different boundaries of 9Cr-steel. Mater Sci Eng A 2004;374:82–9.
[28] Lj Milović. Significance of cracks in the heat-affected-zone of steels for elevated temperature aplication. Struct Integr Life 2008;1:55–65.
[29] Milović Lj. Fissures dans les joints soudés exposés au fluage. Revue électronique internationale pour la science et la technologie [en ligne]. vol. 5; 2010 <http://www.revue-genie-industriel.info/document.php?id=1097>.
[30] Sedmak A, Sedmak S, Milović Lj. Pressure equipment integrity assessment by elastic–plastic fracture mechanics methods. 1st ed. Belgrade: DIVK; 2011.